



Article

Facile and Safe Synthesis of Novel Self-Pored Amine-Functionalized Polystyrene with Nanoscale Bicontinuous Morphology

Qilin Gui ¹, Qi Ouyang ¹, Chunrong Xu ², Hongxue Ding ¹, Shuxian Shi ¹ and Xiaonong Chen ^{1,*}

¹ Beijing Laboratory of Biomaterials, Beijing University of Chemical Technology, Beijing 100029, China; guiql@mail.buct.edu.cn (Q.G.); ouyangqi0000@163.com (Q.O.); Dhx1638170228@163.com (H.D.); shisx@mail.buct.edu.cn (S.S.)

² Key Laboratory of Carbon Fiber and Functional Polymers, Ministry of Education, Beijing University of Chemical Technology, Beijing 100029, China; badwppww@163.com

* Correspondence: chenxn@mail.buct.edu.cn

Received: 16 November 2020; Accepted: 8 December 2020; Published: 10 December 2020



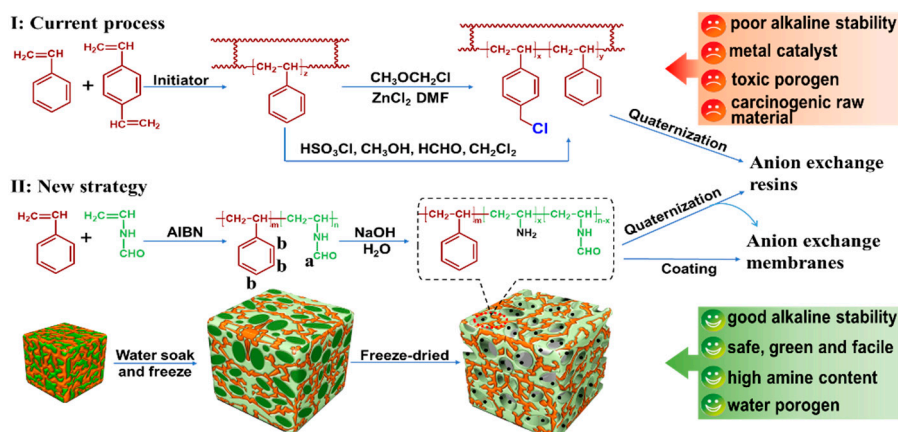
Abstract: The chloromethyl-functionalized polystyrene is the most commonly used ammonium cation precursor for making anion exchange resins (AER) and membranes (AEM). However, the chloromethylation of polystyrene or styrene involves highly toxic and carcinogenic raw materials (e.g., chloromethyl ether) and the resultant ammonium cation structural motif is not stable enough in alkaline media. Herein, we present a novel self-pored amine-functionalized polystyrene, which may provide a safe, convenient, and green process to make polystyrene-based AER and AEM. It is realized by hydrolysis of the copolymer obtained via random copolymerization of *N*-vinylformamide (NVF) with styrene (St). The composition and structure of the NVF-St copolymer could be controlled by monomeric ratio, and the copolymers with high NVF content could form bicontinuous morphology at sub-100 nm levels. Such bicontinuous morphology allows the copolymers to be swollen in water and self-pored by freeze-drying, yielding a large specific surface area. Thus, the copolymer exhibits high adsorption capacity (226 mg/g for bisphenol A). Further, the amine-functionalized polystyrene has all-carbon backbone and hydrophilic/hydrophobic microphase separation morphology. It can be quaternized to produce ammonium cations and would be an excellent precursor for making AEM and AER with good alkaline stability and smooth ion transport channels. Therefore, the present strategy may open a new pathway to develop porous alkaline stable AER and AEM without using metal catalysts, organic pore-forming agents, and carcinogenic raw materials.

Keywords: *N*-vinylformamide; free-radical polymerization; self-pored; functionalized polystyrene; bicontinuous morphology

1. Introduction

Anion exchange resins (AER) and anion exchange membranes (AEM) have always attracted much attention and are widely used in many fields, such as water treatment [1,2], medicine purification [3], microbial or anion exchange membrane fuel cell [4–8], and catalysis. For many decades, benzyltrimethylammonium, which is easily synthesized by quaternization of the chloromethyl-functionalized polystyrene, has been the most commonly used cation in polystyrene-based AEM and AER (Scheme 1) [7,9]. However, this structural motif is not stable enough in alkaline media and can be degraded through β -elimination reaction at the benzyl position [7,10]. In addition, the chloromethylation of polystyrene or styrene involves highly toxic and carcinogenic raw materials (e.g., chloromethyl ether and dichloromethyl ether), which are not environmentally friendly, and has caused many safety concerns [11–13]. In addition, AER and AEM made by this method remain with a number of inherent shortcomings, including poor adjustability of

amino-moiety, self-crosslinking side reaction, potential metal catalyst pollution, and usage of toxic and highly inflammable porogens such as toluene, xylene, dichloroethane, and aliphatic hydrocarbons (Scheme 1I) [12–14]. Therefore, it is necessary to develop a safe and green procedure to make AER and AEM.



Scheme 1. Synthesis and self-poring mechanism of amine-functionalized polystyrene (Current process (I) and new strategy (II) for the preparation of polystyrene-based AER and AEM).

Recently, it has been generally accepted that the all-carbon backbone and alkyltrimethylammonium cations are still the most promising structural motifs for alkaline stable AEM [7,15]. Amine-functionalized polystyrene (PSt-NH₂) may provide an alternative way for manufacturing AEM and AER, since the amine groups on polymer side chains can be easily quaternized. Thus, the PSt-NH₂ prepared by copolymerization of styrene (or styrene derivatives) and *N*-vinylformamide (NVF) may open up a new strategy for green manufacturing of alkaline stable polystyrene-based AER and AEM. On the one hand, NVF units in the copolymer could be easily hydrolyzed to produce amine groups, which are on the polymer side chain and easily converted into alkyltrimethylammonium cations by quaternization [16,17]. The manufacturing process is environmentally friendly, since it involves no metal catalysts, toxic porogens, or carcinogenic raw materials. On the other hand, AEM made by the PS-NH₂ may have good alkaline stability because of its all-carbon backbone structure and alkyltrimethylammonium cations. Although dimethylaminoethyl methacrylate could also provide amine groups, the ester structure is unstable under acidic or basic conditions and the amine group would be easily lost by the hydrolysis of the ester. Further, unlike its isomer acrylamide, NVF is a non-toxic monomer and causes less safety concern [18,19].

Unfortunately, successful random copolymerization of NVF with styrene has rarely been reported, although NVF has high polymerizing reactivity [20], and can randomly copolymerize with vinyl monomers such as acrylic acid, *N*-vinylpyrrolidone, and acrylamide [21,22]. On the one hand, the conjugation effect of styrene is obviously different from that of NVF. The *Q* values of NVF and styrene are 1.0 and 0.29, respectively [23]. Such a large difference in *Q* value increases the difficulty of copolymerization. On the other hand, the polarities of NVF and styrene are so different that only a few solvents could dissolve both monomers and their polymers. Polystyrene microspheres with poly(*N*-vinylformamide) (PNVF) shell were prepared by emulsion polymerization or suspension polymerization [24–26]. However, there was no evidence to show random links between the NVF unit and the styrene unit, and the NVF content in those polymer particles was low (<5%).

In this article, the free-radical copolymerization of styrene and NVF was performed using AIBN as the initiator and DMF as the solvent. We demonstrated for the first time that NVF could randomly copolymerize with styrene. Copolymers with adjustable monomeric composition were successfully obtained via adjusting the monomer feed ratio and monomer concentration. Interestingly, a bicontinuous morphology at sub-100 nm level was found in copolymers with high NVF mass

percentage. Such bicontinuous morphology allowed NVF-St copolymers to be well swollen in water to facilitate the exposure and hydrolysis of NVF units (Figure 1a). Thus, the porous PSt-NH₂ with different amine content was obtained by hydrolysis of NVF-St copolymers. Such PSt-NH₂ could be further quaternized to make polystyrene-based AER and AEM with all-carbon backbone structure and alkyltrimethylammonium cations (Scheme 1II). Additionally, the preparation process did not involve any metal catalyst, toxic porogen, or carcinogenic raw material. Therefore, the preparation of PSt-NH₂ by hydrolyzing the copolymer of styrenic monomers and NVF provided a new strategy for the green production of alkaline and stable polystyrene-based AER and AEM.

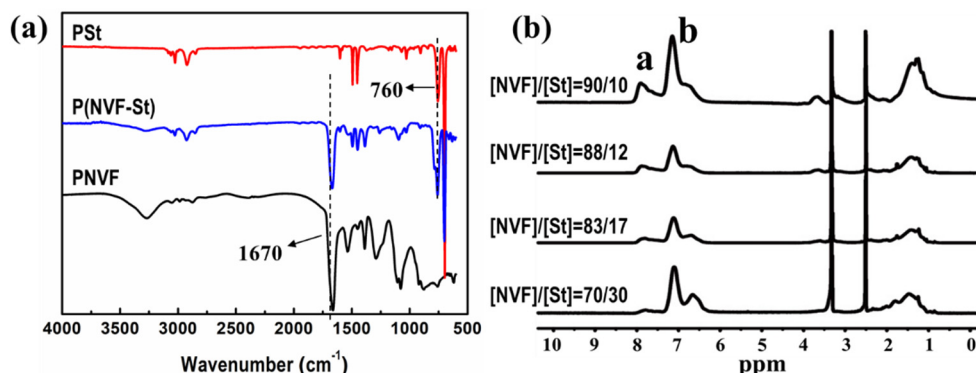


Figure 1. Fourier transform infrared spectroscopy (FTIR) spectra (a) and nuclear magnetic resonance spectroscopy (¹H-NMR) spectra (b) of copolymerizing products.

2. Results and Discussion

2.1. Structure and Composition of the NVF-St Copolymer

Fourier transform infrared spectroscopy (FTIR) and nuclear magnetic resonance spectroscopy (NMR) were conducted to reveal the structure and composition of the copolymerizing products. As shown in Figure 1a, the spectrum of copolymerizing product (P(NVF-St)) showed a strong C = O stretching at 1670 cm⁻¹ and a phenyl ring C-H bending signal at 760 cm⁻¹, which were contributed by NVF and styrene units, respectively [27–29]. In the ¹H-NMR spectra of P(NVF-St) samples (Figure 1b), peak a at 7.5–8.1 and peak b at 6.4–7.3 ppm could be assigned to the protons (1H) of aldehyde group of NVF units and the aromatic protons (5H) of styrene units, respectively [19,30,31]. Thus, both IR and NMR spectra confirmed the formation of NVF-St copolymers.

Moreover, the intensity of peak a showed a positive correlation of NVF content in the copolymer (F_{NVF}) to the NVF monomer content in the polymerization feed (f_{NVF}). Similarly, an increase in the total monomer concentration led to an increase in F_{NVF} (Figure S1). Therefore, copolymers with different NVF content could be obtained by adjusting the f_{NVF} and total monomer concentration. The F_{NVF} was quantitatively calculated according to the intensity of the characteristic peaks a and b in the NMR spectra. As shown in Table 1, although the F_{NVF} was always smaller than f_{NVF} for all the recipes investigated, the F_{NVF} increased alongside the increase of the f_{NVF} , suggesting a statistical model or random style of the copolymerization (Figure S2). The monomer reactivity, r_1 (NVF) and r_2 (St) were roughly estimated to be 0.34 and 10.1, respectively, based on the fitting plot of F_{NVF} against f_{NVF} (Figure S2). According to the Q and e values of the two monomers, the theoretically predicted reactivity r_1 and r_2 were 0.34 and 2.76, respectively [23]. The real monomer reactivity showed some difference from that calculated using Q and e values.

Furthermore, the glass transition temperature (T_g) of the obtained copolymers was measured by differential scanning calorimetry (DSC), which could be used to distinguish random copolymers from polymer blends and block copolymers. Generally, only a single T_g could be detected for the homo-polymer or random copolymer, while two or more T_g values could be observed for blended polymers or block copolymers [32]. As shown in Figure 2a, the homo-polystyrene (PSt) exhibited a

glass transition around 95 °C, while the PNVF was around 142 °C. There were two T_g values at about 95 and 142 °C in the DSC curve of the PNVF/PSt blend (Figure 2a), corresponding to PSt and PNVF, respectively. Notably, Figure 2b and Figure S3 show that only one T_g appeared in each DSC curve of the copolymer samples. These results obtained from glass transition measurement confirmed random architecture of the NVF-St copolymers. Table 1 provides all T_g values of the copolymers, showing that the T_g of the copolymer increased with the increase of the F_{NVF} . Thus, the Fox equation [32,33], which is an empirical formula to describe the linear dependence of the glass transition temperature of a random copolymer on its composition, was used to reveal the relationship between the T_g and the composition of the NVF-St copolymers.

$$\frac{1}{T_g} = \left(\frac{1}{T_{gA}} - \frac{1}{T_{gB}} \right) \omega_A + \frac{1}{T_{gB}} \quad (1)$$

where, T_{gA} , T_{gB} , and T_g are the glass transition temperatures of PNVF (142 °C), PSt (95 °C), and NVF-St copolymer, respectively, and ω_A is the mass percentage of NVF unit in the copolymers (F_{NVF}). Figure 2c presents the plot of T_g^{-1} against the $\omega_A (F_{\text{NVF}})$. The experimental plot showed good linearity (with a correlation coefficient of 0.9906) and was close to the plot using the Fox equation. This result well demonstrated random architecture of the NVF and St units composing the copolymer. Notably, the T_g of NVF-St copolymer was larger than that of PSt, suggesting a better heat resistance of the functionalized polystyrene than the homo-polystyrene. In the future, we may prepare copolymers with higher glass transition temperature and good heat resistance through copolymerization of styrene derivatives and NVF.

Table 1. Composition and T_g of *N*-vinylformamide (NVF-St) copolymers *.

No.	Molar Ratio of NVF/St	NVF Mass Percentage in Monomer Feed, f_{NVF} (%)	Total Monomer Concentration (Wt%)	NVF Mass Percentage in Product (by NMR), F_{NVF} (%)	T_g of Product (°C)
1	70/30	61.4	20	15.2	106
2	83/17	77.3	20	37.4	118
3	88/12	82.7	20	46.7	121
4	90/10	86.0	20	51.7	125
5	83/17	77.3	30	47.6	123
6	83/17	77.3	40	58.0	129

* The copolymerization was performed at 60 °C for 10 h using azodiisobutyronitrile (AIBN) as initiator.

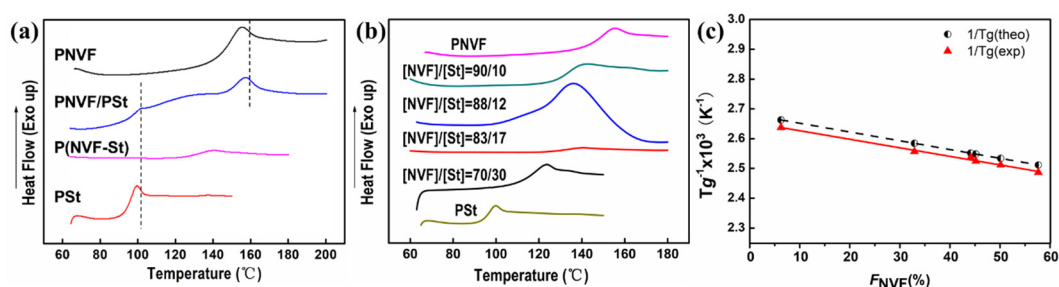


Figure 2. DSC curves of (a) PNVF/PSt blend (mass ratio 1/1) and (b) NVF-St copolymers. (c) The relationship between T_g and NVF unit content in NVF-St copolymers. Solid triangle dot: T_g obtained by DSC measurement; cycle dot: T_g calculated based on the composition using Fox equation.

2.2. Microphase Separation Morphology of the NVF-St Copolymer

Styrene is known as the most commonly used hydrophobic monomer, while NVF is a hydrophilic functional monomer [21]. Thus, a hydrophobic phase (dominated by styrene units) and a hydrophilic phase (dominated by NVF units) could be formed in an interpenetrating morphology [6].

Similarly, phase-separated co-network morphology was observed in the case of copolymer of poly(dimethylsiloxane)- α,ω -diacrylate and N,N-dimethylacrylamide [34]. It seems that the significant difference in polarity of the two monomeric moieties is responsible for the immiscibility at the microscale. To visually study the morphology of the sample, atomic force microscopy (AFM) was used. AFM images confirmed that the NVF-St copolymer underwent phase separation and formed a two-phase bicontinuous structure with non-long-range ordering, when the F_{NVF} became larger than 50% (Figure 3). Note that the size of the bicontinuous morphology was sub-100 nm, which was much smaller than the classical one formed by block copolymers or blends [35,36]. This may have been caused by the random distribution of NVF and styrene units, which prevented the growth of both hydrophobic and hydrophilic phases by forming an interpenetrated phase separation morphology.

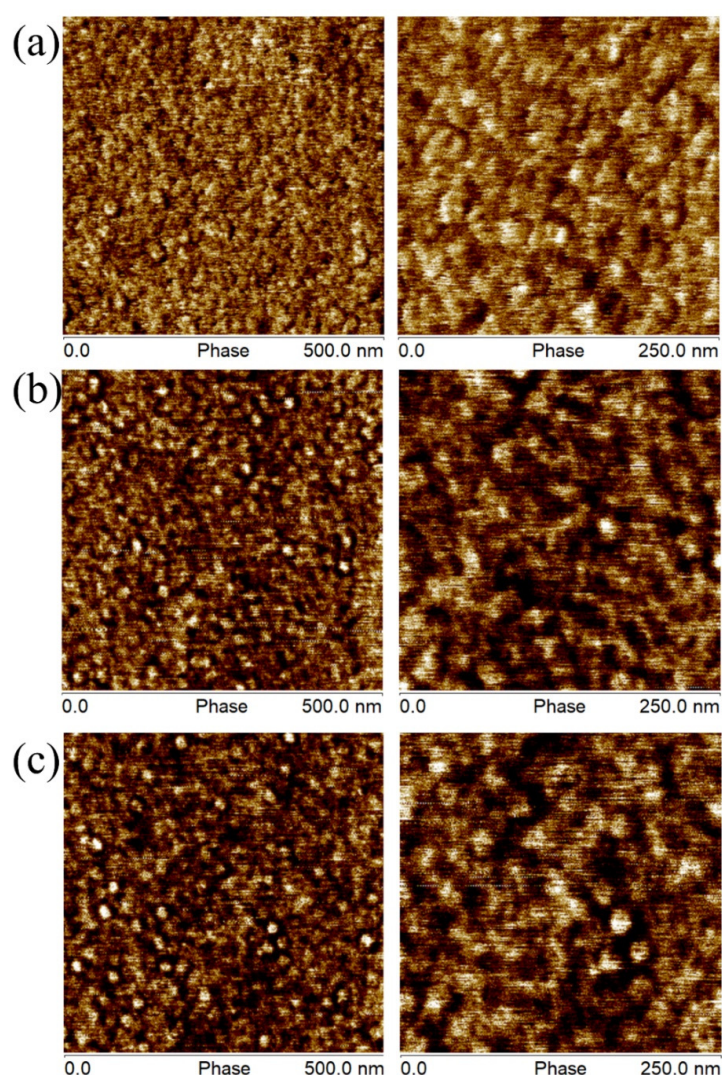


Figure 3. Atomic force microscopy (AFM) images (recorded on the thin film prepared through spin-coating) of (a) NVF-St-37.4 (No.2), (b) NVF-St-51.7 (No.4), and (c) NVF-St-58 (No.6).

To further verify the microphase separation structure of the copolymer, transmission electron microscopy (TEM) was used. The copolymer samples were annealed at 120 °C for 3 h, and dyed by reaction of $-\text{NH}-\text{CHO}$ groups in NVF units with RuO_4 . Figure 4 shows that as the F_{NVF} increased, the area of the dark black zone became larger, indicating that the hydrophilic phase dominated by NVF increased. Moreover, when the F_{NVF} increased from 37.4% to 58.0%, the copolymer underwent a phase transition and formed a microphase separation morphology. The NVF-St-58.0 exhibited obvious an microphase separation phenomenon between a hydrophilic phase dominated by NVF

units (dark black) and a hydrophobic phase dominated by styrene units (light gray) due to the self-assembly behavior from two different kinds of incompatible segments in the copolymer. In the TEM images, the characteristic size of the microphase separation structure was about 40 nm, which was consistent with the results of AFM. It is worth mentioning that there were dense black spots at the hydrophilic phase and the hydrophilic/hydrophobic phase interface, indicating that the NVF side groups (-NH-CHO) in the copolymer could be exposed in water. Thus, the bicontinuous morphology may have facilitated the exposure and hydrolysis of NVF units to generate amine groups, which was essential for the preparation of amine-functionalized polystyrene. In addition, the good film-forming performance of the NVF-St copolymer allowed it to be possible to prepare the copolymer membrane, which could be converted into PSt-NH₂ membrane by hydrolysis and further converted into AEM through quaternization.

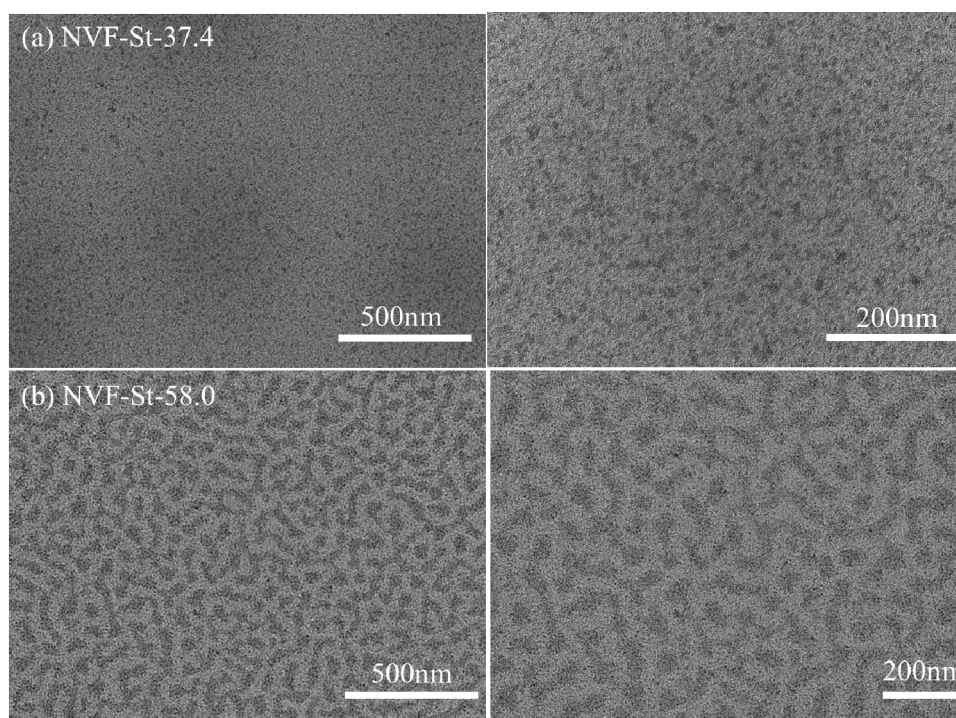


Figure 4. Transmission electron microscopy (TEM) images of (a) NVF-St-37.4 (No.2) and (b) NVF-St-58 (No.6) dyed with RuO₄.

2.3. Hydrolysis, Quaternization, and Potential Applications of the NVF-St Copolymer

The hydrolysis and further quaternization of the NVF-St copolymer were carried out. Comparing the IR spectra of P(NVF-St) and PSt-NH₂, it was found that a strong amine absorption peak appeared at 1452 cm⁻¹, while the aldehyde absorption peak at 1670 cm⁻¹ almost disappeared (Figure 5a). This indicated that NVF-St copolymers could easily hydrolyze under basic conditions to produce PSt-NH₂ (Scheme 1II). The resultant PSt-NH₂ could be quaternized using bromoethane under the mild condition, as shown by the peak at 1114 cm⁻¹, corresponding to the C-N bond of quaternary ammonium in the IR spectra (Figure 5a) [28,37]. It is known that a quaternary ammonium containing benzyl is not stable under strong alkali conditions due to β -elimination reaction [7]. Compared with ammonium cations prepared from chloromethyl-functionalized polystyrene, the alkyltrimethylammonium cations prepared based on the PSt-NH₂ may have had better alkaline stability because the resultant quaternary ammonium moieties did not contain benzyl group. Moreover, the all-carbon skeleton structure could also improve the alkaline stability of AEM and AER [15]. Therefore, the PSt-NH₂ could be used as the precursor for making alkaline stable polystyrene-based AER and AEM.

Functionalized polystyrene is a commonly used adsorbent; thus, it is worth evaluating the adsorption performance of the NVF-St copolymers before and after hydrolysis. Bisphenol A (BPA), which has been intensively concerned as an endocrine disruptor [38], was selected as a model pollutant. Figure 5b,c shows that the BPA uptake (mg/g) of the NVF-St copolymer significantly increased when the F_{NVF} reached 50%. This is because the NVF-St copolymer underwent a phase separation and formed a bicontinuous morphology at the specific F_{NVF} . The bicontinuous morphology allowed the NVF-St copolymer to be swollen in water and self-pored by freeze-drying. Therefore, the freeze-dried copolymer provided improved adsorption performance (Figure 5b). The mechanism of self-poring by the freeze-drying process is shown in Scheme 1. The hydrophilic phase dominated by NVF units in the copolymer sample absorbed and swelled in water. The absorbed water was frozen and removed during freeze drying, leading to the formation of pores. In such a case, water serves as a pore-forming agent. Compared with organic porogens, water is a safe and cheap porogen, which may provide a green and safe pore-forming process.

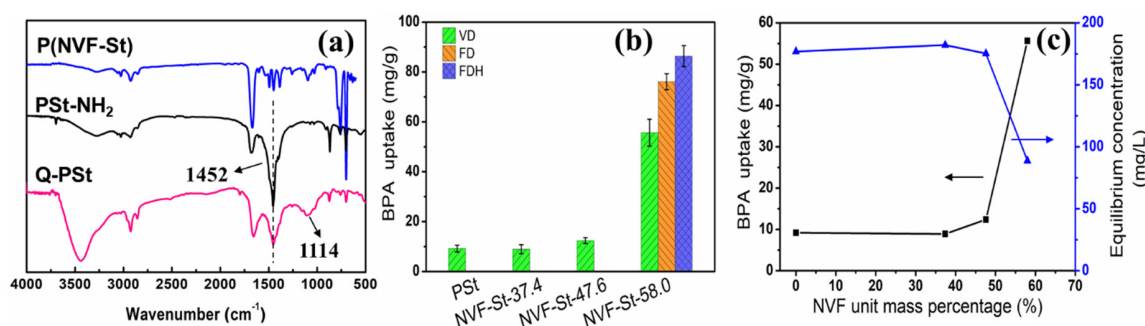


Figure 5. (a) FTIR spectra of P(NVF-St), PSt-NH₂, and quaternized sample(Q-PSt). (b) Bisphenol A (BPA) uptake (mg/g) of NVF-St copolymers (VD: Vacuum-dried, FD: Freeze-dried, FDH: Hydrolyzed, dialyzed, and freeze-dried) and (c) the relationship between BPA uptake and NVF unit content in NVF-St copolymers (vacuum-dried). Adsorption condition: Copolymer 10 mg, BPA 200 mg/L, 5 mL, pH 7, 18 h, room temperature.

Scanning electron microscopy (SEM) and Brunauer–Emmett–Teller (BET) analysis were used to observe the formation of holes. SEM images (Figure 6) and the significant increase in specific surface area (Table S1) also demonstrated the formation of through-holes, which was related to the hydrophilic–hydrophobic bicontinuous morphology. According to Figure 6a,b, the sample (No.6) prepared under vacuum-dried had smooth and continuous surface morphology, while after freeze-drying, the morphology became porous and rough. Therefore, the specific surface area (Table S1) of the latter (80.5 m²/g) was much larger than that of the former (3.5 m²/g). The specific surface area directly affected the adsorption performance. In future study, the pore morphology and specific surface area of the NVF-St copolymer may be further well controlled by adjusting the conditions such as the freezing rate. Most importantly, the bicontinuous morphology facilitated the exposure and hydrolysis of NVF units to generate amine groups (Figure 5a). After hydrolysis, the sample (No.6) showed the highest BPA uptake (as high as 86 mg/g and about 8.5 times larger than that of PSt, Figure 5b). The hydrolyzed product not only had a porous structure (Figure 6c), but also provided an additional positive charge to interact with the phenol group in BPA. Additionally, the increase of the BPA equilibrium concentration could further improve the BPA uptake of the sample. When the equilibrium concentration was increased to 0.5 mmol/L, the BPA uptake of the hydrolyzed product reaches 226 mg/g. Compared with commonly used activated carbon and polymer adsorbents (Table 2), NVF-St copolymer had higher adsorption capacity and could be prepared in a facile way by free radical copolymerization. Therefore, the strategy of free-radical copolymerization of NVF with styrene may be used to obtain PSt-NH₂ in a simple way. In short, the resultant PSt-NH₂ was a desirable precursor for making AER and AEM, because it had adjustable water uptake, obvious microphase separation structure, and green and facile preparation process.

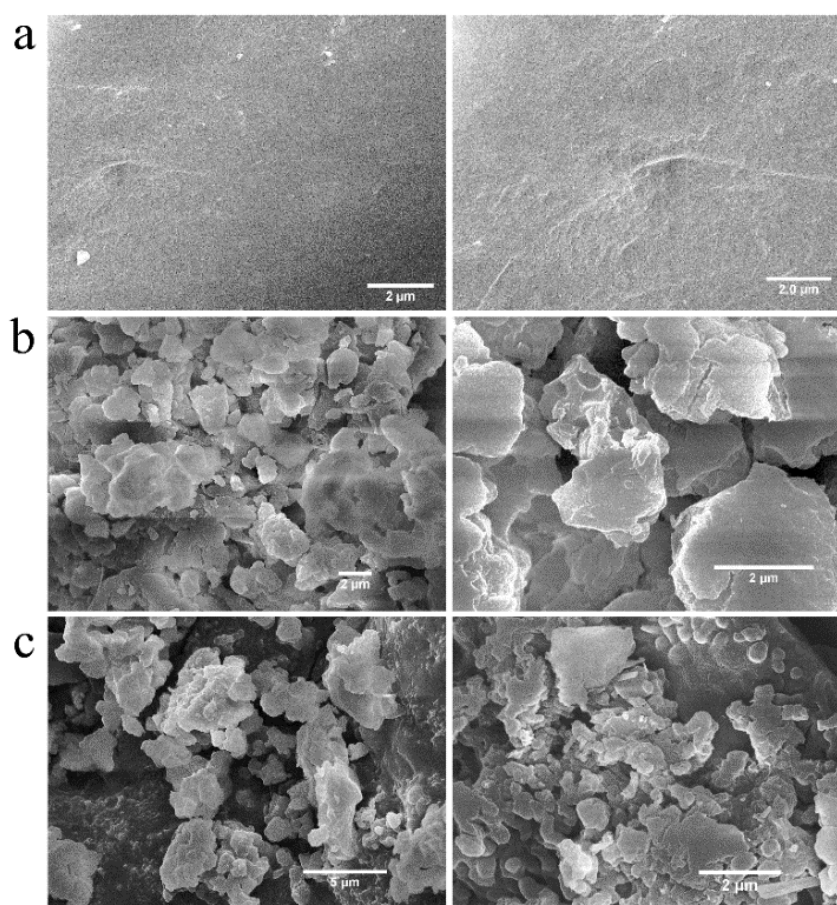


Figure 6. SEM images of NVF-St copolymer sample (No.6) prepared under different drying conditions. (a) Vacuum-dried; (b) freeze-dried; and (c) hydrolyzed, dialyzed, and freeze-dried.

Table 2. Comparison of BPA adsorption capacity of the copolymer with commonly used activated carbon and polymer adsorbents reported in the literature.

Adsorbent	q_e (mg/g)	Year/Ref.
HAP membranes	129.4	2017 [39]
β -cyclodextrin polymers on microcrystalline cellulose	34.7	2019 [40]
Magnetic vermiculite-modified by poly(trimesoyl chloride-melamine)	217.4	2019 [41]
Porous β -cyclodextrin/pillar[5]arene copolymer	78.9	2019 [42]
Porous β -cyclodextrin polymer	88	2016 [43]
Highly water stable graphene oxide-based composites	13.2	2019 [44]
Magnetic reduced graphene oxides	58.2	2015 [45]
Consumer-grade polyurethane foam	268	2015 [46]
Graphene	10	2017 [47]
Reduced graphene oxide	365	2017 [48]
Organo-acid-activated bentonite	127.7	2017 [49]
Electrospun nylon 6,6 membrane	91.3	2017 [50]
Hydrophobic magnetic montmorillonite composite material	59.2	2016 [51]
Mesoporous $\text{CaSiO}_3@SiO_2$ grafted nonwoven polypropylene fiber	55	2017 [52]
Crosslinked β -cyclodextrin polymer	113	2017 [53]
The NVF-St copolymer (containing 58% of NVF unit)	226	This work

3. Materials and Methods

3.1. Materials and Instrumentations

Materials and instrumentations are shown in the electronic supplementary information (ESI), Sections S1 and S2. *N*-vinylformamide (NVF) (Aldrich) and styrene (St) (Beijing Chemical Works,

Beijing, China) were purified by distillation under reduced pressure. The structure and composition of the NVF-St copolymer were characterized by Fourier transform infrared spectroscopy (FTIR), nuclear magnetic resonance spectroscopy (NMR), differential scanning calorimetry (DSC), and gel permeation chromatography (GPC). The morphology and self-poring mechanism were revealed by atomic force microscope (AFM), transmission electron microscope (TEM), scanning electron microscopy (SEM), and Brunauer–Emmett–Teller (BET) analysis. The DMSO solution of NVF-St copolymer (1–3 mg/mL) was dropped on a silicon wafer to form a film by KW4A spin coater at 3000 r/min for 60 s. Samples were annealed at 120 °C for three hours before testing AFM. UV-visible spectroscopy was used to determine the concentration of BPA in solution.

3.2. Experimental Procedure

3.2.1. Copolymerization of NVF and St

The copolymerization was performed under nitrogen atmosphere at 60 °C in a 50-mL sealed flask for 10 h using AIBN (1.5% of the total mass of the monomers) as the initiator and DMF as the solvent. Different mass ratios of monomers ((NVF)/(St) were 70/30, 83/17, 88/12, 90/10, respectively) were employed and the total monomer concentration controlled as 20%, 30%, or 40%. The copolymerizing product was dissolved in a mixed solvent of DMSO and water in a volume ratio of DMSO/water at 3/1. Then ethanol was added into the solution to obtain polymer precipitation. Such dissolution/precipitation was repeated three times. The resultant final precipitate was vacuum-dried or freeze-dried until a constant weight was reached, to obtain pure copolymer (yield 30–50%). The molecular weight of the copolymer (No.1) was found to be around 12 kDalton (Figure S4).

3.2.2. Hydrolysis of the NVF-St Copolymer

The copolymer was hydrolyzed to obtain polyvinylamine. Typically, in a flask, 4.0 g of the copolymer (No.6) was mixed with 15 mL of water and 35 mL of 5% aqueous NaOH solution. The mixture was magnetically stirred and heated in a 60 °C oil bath for 24 h. The resultant solution was neutralized to pH 7.0 using 1 mol/L HCl aqueous solution, followed by dialyzing and freeze-dried to obtain 2.9 g product (the degree of hydrolysis: 85%).

3.2.3. Quaternization of the Hydrolyzed Copolymer

Typically, in a flask, 1.4 g hydrolyzed copolymer (No.6), 8.6 g bromoethane, and 6.3 g Na₂CO₃ were mixed with 30 mL water and 30 mL DMSO. The mixture was magnetically stirred and heated in a 60 °C oil bath for 8 h. The resultant solution was neutralized using 1 mol/L HCl aqueous solution. Then ethanol was added into the mixture to obtain polymer precipitation. The polymer precipitation was dialyzed and freeze-dried to obtain 1.2 g product.

3.2.4. Batch Adsorption Experiments

Adsorption studies were performed in 10-mL centrifuge tubes equipped with a magnetic stir bar (the stirring rate is 150 r.p.m.) at ambient temperature. The NVF-St copolymer (10 mg) was added into 5 mL of BPA solution (200 mg/L, pH 7) for 18 h. Then, the mixture was filtered by a PTFE (0.2 µm) membrane, and the residual concentration of BPA in each sample was determined by UV-visible spectroscopy. The amount of BPA bound to the copolymer (Q_m) was calculated by the following equation:

$$Q_m = \frac{(C_o - C_e) \times V}{m_c} \quad (2)$$

where C_o and C_e are the BPA concentrations in solution before and after adsorption, respectively, V is the volume of the solution, and m_c is the mass of the copolymer.

4. Conclusions

In summary, NVF-St copolymers with different NVF contents were synthesized via free-radical copolymerization in a simple way by adjusting the monomer feed ratio and monomer concentration. The bicontinuous morphology with a size at sub-100 nm level was formed in the NVF-St copolymers with high NVF mass percentage. Such a structure allowed NVF-St copolymers to be self-pored by water-swelling and freeze-drying, resulting in a large specific surface area. The BPA uptake of the copolymer reached 226 mg/g, which was larger than that of the commonly used activated carbon and polymer adsorbents, indicating the copolymer has higher adsorption capacity. Additionally, the NVF-St copolymer was easily hydrolyzed to convert into amine-functionalized polystyrene, which could be further quaternized to produce ammonium cations. The amine-functionalized polystyrene would be an excellent precursor for making polystyrene-based AER and AEM with all-carbon backbone structure and benzyl-free quaternary ammonium and smooth ion transport channels. The entire process, from the copolymerization, hydrolysis, to the quaternization, did not involve any metal catalyst, toxic porogen, or carcinogenic raw material. Therefore, the process may provide a safe, green, and facile way to access AER and AEM. Prospectively, AER and AEM made by the amine-functionalized polystyrene may have potential applications in many fields, such as anion exchange membrane fuel cell, adsorbent materials, catalysts, water treatment, and drug separation/purification.

Supplementary Materials: Supplementary materials can be found at <http://www.mdpi.com/1422-0067/21/24/9404/s1>.

Author Contributions: Data curation, Q.G. and Q.O.; investigation, Q.G. and H.D.; writing—original draft preparation, Q.G. and C.X.; writing—review and editing, S.S. and X.C.; funding acquisition, X.C. All authors have read and agreed to the published version of the manuscript.

Funding: This research was funded by the National Science Foundation of China (Grant No. 51573211).

Acknowledgments: The authors would like to thank the National Natural Science Foundation of China (Grant No. 51573211) for financial support. Robert Peltion, Department of Chemical Engineering at McMaster University, Canada, is highly appreciated for valuable discussion.

Conflicts of Interest: The authors declare no conflict of interest.

References

1. Bui, T.H.; Hong, S.P.; Yoon, J. Development of nanoscale zirconium molybdate embedded anion exchange resin for selective removal of phosphate. *Water Res.* **2018**, *134*, 22–31. [[CrossRef](#)] [[PubMed](#)]
2. Mondal, S.; Majumder, S.K. Fabrication of the polysulfone-based composite ultrafiltration membranes for the adsorptive removal of heavy metal ions from their contaminated aqueous solutions. *Chem. Eng. J.* **2020**, *401*, 126036. [[CrossRef](#)]
3. Landry, K.A.; Sun, P.; Huang, C.-H.; Boyer, T.H. Ion-exchange selectivity of diclofenac, ibuprofen, ketoprofen, and naproxen in ureolyzed human urine. *Water Res.* **2015**, *68*, 510–521. [[CrossRef](#)] [[PubMed](#)]
4. Zeppilli, M.; Lai, A.; Villano, M.; Majone, M. Anion vs. cation exchange membrane strongly affect mechanisms and yield of CO₂ fixation in a microbial electrolysis cell. *Chem. Eng. J.* **2016**, *304*, 10–19. [[CrossRef](#)]
5. Hernández-Fernández, F.; Ríos, A.P.D.L.; Mateo-Ramírez, F.; Godínez, C.; Lozano-Blanco, L.; Moreno, J.I.; Tomás-Alonso, F. New application of supported ionic liquids membranes as proton exchange membranes in microbial fuel cell for waste water treatment. *Chem. Eng. J.* **2015**, *279*, 115–119. [[CrossRef](#)]
6. Liu, D.; Xu, M.; Fang, M.; Chen, J.; Wang, L. Branched comb-shaped poly(arylene ether sulfone)s containing flexible alkyl imidazolium side chains as anion exchange membranes. *J. Mater. Chem. A* **2018**, *6*, 10879–10890. [[CrossRef](#)]
7. You, W.; Noonan, K.J.; Coates, G.W. Alkaline-stable anion exchange membranes: A review of synthetic approaches. *Prog. Polym. Sci.* **2020**, *100*, 101177. [[CrossRef](#)]
8. Fang, M.; Liu, D.; Neelakandan, S.; Xu, M.; Liu, D.; Wang, L. Side-chain effects on the properties of highly branched imidazolium-functionalized copolymer anion exchange membranes. *Appl. Surf. Sci.* **2019**, *493*, 1306–1316. [[CrossRef](#)]

9. Merle, G.G.; Wessling, M.M.; Nijmeijer, D.C. Anion exchange membranes for alkaline fuel cells: A review. *J. Membr. Sci.* **2011**, *377*, 1–35. [[CrossRef](#)]
10. Yang, K.; Xu, J.; Shui, T.; Zhang, Z.; Wang, H.; Liu, Q.; Chen, W.; Shen, H.; Zhang, H.; Yang, D.; et al. Cross-linked poly (aryl ether ketone) anion exchange membrane with high ion conductivity by two different functional imidazole side chain. *React. Funct. Polym.* **2020**, *151*, 104551. [[CrossRef](#)]
11. Seliman, A.F.; Samadi, A.; Husson, S.M.; Borai, E.H.; DeVol, T.A. Preparation of polymer-coated, scintillating ion-exchange resins for monitoring of ⁹⁹Tc in groundwater. *Anal. Chem.* **2011**, *83*, 4759–4766. [[CrossRef](#)]
12. Yao, P.; Huang, Z.; Zhu, Q.; Zhu, Z.; Wang, L.; Zhu, Y. A novel composite stationary phase composed of polystyrene/divinylbenzene beads and quaternized nanodiamond for anion exchange chromatography. *Chin. Chem. Lett.* **2019**, *30*, 465–469. [[CrossRef](#)]
13. Cyganowski, P.; Cierlik, A.; Leśniewicz, A.; Pohl, P.; Jermakowicz-Bartkowiak, D. Separation of Re(VII) from Mo(VI) by anion exchange resins synthesized using microwave heat. *Hydrometallurgy* **2019**, *185*, 12–22. [[CrossRef](#)]
14. Fu, Y.; Huang, X.; Zhong, S.; Yi, W.-J.; Li, L.-J. A new chloromethylation method based on polystyrene-divinylbenzene. *Chem. Pap.* **2019**, *73*, 2183–2188. [[CrossRef](#)]
15. Park, E.J.; Kim, Y.S. Quaternized aryl ether-free polyaromatics for alkaline membrane fuel cells: Synthesis, properties, and performance—a topical review. *J. Mater. Chem. A* **2018**, *6*, 15456–15477. [[CrossRef](#)]
16. Pinschmidt, R.K. Polyvinylamine at last. *J. Polym. Sci. Part A Polym. Chem.* **2010**, *48*, 2257–2283. [[CrossRef](#)]
17. Pelton, R. Polyvinylamine: A Tool for Engineering Interfaces. *Langmuir* **2014**, *30*, 15373–15382. [[CrossRef](#)]
18. Shi, L.; Berkland, C. pH-triggered dispersion of nanoparticle clusters. *Adv. Mater.* **2006**, *18*, 2315–2319. [[CrossRef](#)]
19. Marhefka, J.N.; Marascalco, P.J.; Chapman, T.M.; Russell, A.; Kameneva, M.V. Poly(N-vinylformamide)A Drag-Reducing Polymer for Biomedical Applications. *Biomacromolecules* **2006**, *7*, 1597–1603. [[CrossRef](#)]
20. Gu, L.; Zhu, S.; Hrymak, A.N.; Pelton, R.H. Kinetics and modeling of free radical polymerization of N-vinylformamide. *Polymer* **2001**, *42*, 3077–3086. [[CrossRef](#)]
21. Chang, Y.; McCormick, C.L. Water-soluble copolymers. 47. Copolymerization of maleic anhydride and N-vinylformamide. *Macromolecules* **1993**, *26*, 4814–4817. [[CrossRef](#)]
22. Santuryan, Y.G.; Malakhova, I.I.; Gorshkov, N.I.; Krasikov, V.D.; Panarin, E.F. Water-soluble poly(n-vinylamides) as a basis for the synthesis of polymeric carriers of biologically active compounds. *Int. J. Polym. Anal. Charact.* **2019**, *24*, 105–113. [[CrossRef](#)]
23. Gu, L.; Zhu, S.; Hrymak, A.N. Modeling molecular weight distribution of comb-branched graft copolymers. *J. Polym. Sci. Part B Polym. Phys.* **1998**, *36*, 705–714. [[CrossRef](#)]
24. Shevchenko, N.; Pankova, G.A.; Evseeva, T.G.; Shabsel'S, B.M.; Baigil'Din, V.A.; Men'Shikova, A.Y. Copolymerization of styrene with N-vinylformamide and ethylene glycol dimethacrylate and characteristics of the formed particles. *Polym. Sci. Ser. B* **2014**, *56*, 132–138. [[CrossRef](#)]
25. Menshikova, A.; Evseeva, T.; Shevchenko, N.; Shabsels, B.; Yakimansky, A.V.; Ivanchev, S.S. Monodisperse Particles Based on Copolymers of Methyl methacrylate or Styrene with N-Vinylformamide. *Macromol. Symp.* **2009**, *281*, 61–68. [[CrossRef](#)]
26. Xu, J.; Timmons, A.B.; Pelton, R. N -Vinylformamide as a route to amine-containing latexes and microgels. *Colloid Polym. Sci.* **2004**, *282*, 256–263. [[CrossRef](#)]
27. Jeon, C.; Kim, D.W.; Chang, S.; Kim, J.G.; Seo, M. Synthesis of Polypropylene via Catalytic Deoxygenation of Poly(methyl acrylate). *ACS Macro Lett.* **2019**, *8*, 1172–1178. [[CrossRef](#)]
28. Alikhani, M.; Moghbeli, M. Ion-exchange polyHIPE type membrane for removing nitrate ions: Preparation, characterization, kinetics and adsorption studies. *Chem. Eng. J.* **2014**, *239*, 93–104. [[CrossRef](#)]
29. Zhang, L.; Li, L.; Wang, L.; Nie, J.; Ma, G. Multilayer electrospun nanofibrous membranes with antibacterial property for air filtration. *Appl. Surf. Sci.* **2020**, *515*, 145962. [[CrossRef](#)]
30. Chakraborty, S.; Ramakrishnan, S. Surface-Functionalized Polystyrene Latexes Using Itaconate-Based Surfmers. *Langmuir* **2018**, *34*, 11729–11737. [[CrossRef](#)]
31. Yang, L.; Ma, H.; Han, L.; Hao, X.; Liu, P.; Shen, H.; Li, Y. Synthesis of a sequence-controlled in-chain alkynyl/tertiary amino dual-functionalized terpolymers via living anionic polymerization. *Polym. Chem.* **2018**, *9*, 108–120. [[CrossRef](#)]
32. Brostow, W.; Chiu, R.; Kalogeras, I.M.; Vassilikou-Dova, A. Prediction of glass transition temperatures: Binary blends and copolymers. *Mater. Lett.* **2008**, *62*, 3152–3155. [[CrossRef](#)]

33. Park, C.H.; Kim, J.H.; Ree, M.; Sohn, B.; Jung, J.C.; Zin, W. Thickness and composition dependence of the glass transition temperature in thin random copolymer films. *Polymer* **2004**, *45*, 4507–4513. [[CrossRef](#)]
34. Yamamoto, K.; Ito, E.; Fukaya, S.; Takagi, H. Phase-separated conetwork structure induced by radical copolymerization of poly(dimethylsiloxane)- α,ω -diacrylate and N,N-dimethylacrylamide. *Macromolecules* **2009**, *42*, 9561–9567. [[CrossRef](#)]
35. Nofar, M.; Maani, A.; Sojoudi, H.; Heuzey, M.; Carreau, P.J. Interfacial and rheological properties of PLA/PBAT and PLA/PBSA blends and their morphological stability under shear flow. *J. Rheol.* **2015**, *59*, 317–333. [[CrossRef](#)]
36. Ren, D.; Tu, Z.; Yu, C.; Shi, H.; Jiang, T.; Yang, Y.; Shi, D.; Yin, J.; Mai, Y.-W.; Li, R.K. Effect of Dual Reactive Compatibilizers on the Formation of Co-Continuous Morphology of Low Density Polyethylene/Polyamide 6 Blends with Low Polyamide 6 Content. *Ind. Eng. Chem. Res.* **2016**, *55*, 4515–4525. [[CrossRef](#)]
37. Han, S.; Zang, Y.; Gao, Y.; Yue, Q.; Zhang, P.; Kong, W.; Jin, B.; Xu, X.; Gao, B. Co-monomer polymer anion exchange resin for removing Cr(VI) contaminants: Adsorption kinetics, mechanism and performance. *Sci. Total Environ.* **2020**, *709*, 136002. [[CrossRef](#)] [[PubMed](#)]
38. Gui, Q.; Zhang, J.; Hu, K.; Ouyang, Q.; Shi, S.; Chen, X. Hydrogen bonding-induced hydrophobic assembly yields strong affinity of an adsorptive membrane for ultrafast removal of trace organic micropollutants from water. *J. Mater. Chem. A* **2020**, *8*, 16487–16496. [[CrossRef](#)]
39. He, J.; Li, Y.; Cai, X.; Chen, K.; Zheng, H.; Wang, C.; Zhang, K.; Lin, D.; Kong, L.; Liu, J. Study on the removal of organic micropollutants from aqueous and ethanol solutions by HAP membranes with tunable hydrophilicity and hydrophobicity. *Chemosphere* **2017**, *174*, 380–389. [[CrossRef](#)]
40. Alzate-Sánchez, D.M.; Ling, Y.; Li, C.; Frank, B.P.; Bleher, R.; Fairbrother, H.; Helbling, D.E.; Dichtel, W.R. β -Cyclodextrin Polymers on Microcrystalline Cellulose as a Granular Media for Organic Micropollutant Removal from Water. *ACS Appl. Mater. Interfaces* **2019**, *11*, 8089–8096. [[CrossRef](#)]
41. Saleh, T.A.; Tuzen, M.; Sari, A. Magnetic vermiculite-modified by poly(trimesoyl chloride-melamine) as a sorbent for enhanced removal of bisphenol A. *J. Environ. Chem. Eng.* **2019**, *7*, 103436. [[CrossRef](#)]
42. Lu, P.; Cheng, J.; Li, Y.; Li, L.; Wang, Q.; He, C. Novel porous β -cyclodextrin/pillar[5]arene copolymer for rapid removal of organic pollutants from water. *Carbohydr. Polym.* **2019**, *216*, 149–156. [[CrossRef](#)] [[PubMed](#)]
43. Alsaiee, A.; Smith, B.J.; Xiao, L.; Ling, Y.; Helbling, D.E.; Dichtel, W.R. Rapid removal of organic micropollutants from water by a porous β -cyclodextrin polymer. *Nature* **2016**, *529*, 190–194. [[CrossRef](#)] [[PubMed](#)]
44. Delhiraja, K.; Vellingiri, K.; Boukhvalov, D.W.; Philip, L. Development of Highly Water Stable Graphene Oxide-Based Composites for the Removal of Pharmaceuticals and Personal Care Products. *Ind. Eng. Chem. Res.* **2019**, *58*, 2899–2913. [[CrossRef](#)]
45. Jin, Z.; Wang, X.; Sun, Y.; Ai, Y.; Wang, X. Adsorption of 4-n-Nonylphenol and Bisphenol-A on Magnetic Reduced Graphene Oxides: A Combined Experimental and Theoretical Studies. *Environ. Sci. Technol.* **2015**, *49*, 9168–9175. [[CrossRef](#)] [[PubMed](#)]
46. Han, J.; Qiu, W.; Tiwari, S.; Bhargava, R.; Gao, W.; Xing, B. Consumer-grade polyurethane foam functions as a large and selective absorption sink for bisphenol A in aqueous media. *J. Mater. Chem. A* **2015**, *3*, 8870–8881. [[CrossRef](#)]
47. Wang, F.; Lu, X.; Peng, W.; Deng, Y.; Zhang, T.; Hu, Y.-B.; Li, X.-Y. Sorption Behavior of Bisphenol A and Triclosan by Graphene: Comparison with Activated Carbon. *ACS Omega* **2017**, *2*, 5378–5384. [[CrossRef](#)]
48. Wang, X.; Tang, P.; Ding, C.; Cao, X.; Yuan, S.; Zuo, X.; Deng, X. Simultaneous enhancement of adsorption and peroxymonosulfate activation of Nitrogen-doped reduced graphene oxide for bisphenol A removal. *J. Environ. Chem. Eng.* **2017**, *5*, 4291–4297. [[CrossRef](#)]
49. Djebri, N.; Boutahala, M.; Chelali, N.-E.; Boukhalfa, N.; Larbi, Z. Adsorption of bisphenol A and 2,4,5-trichlorophenol onto organo-acid-activated bentonite from aqueous solutions in single and binary systems. *Desalin. Water Treat.* **2017**, *66*, 383–395. [[CrossRef](#)]
50. Jasni, M.J.F.; Arulkumar, M.; Sathishkumar, P.; Yusoff, A.R.M.; Buang, N.A.; Gu, F. Electrospun nylon 6,6 membrane as a reusable nano-adsorbent for bisphenol A removal: Adsorption performance and mechanism. *J. Colloid Interface Sci.* **2017**, *508*, 591–602. [[CrossRef](#)]
51. Salehinia, S.; Ghoreishi, S.M.; Maya, F.; Cerdà, V. Hydrophobic magnetic montmorillonite composite material for the efficient adsorption and microextraction of bisphenol A from water samples. *J. Environ. Chem. Eng.* **2016**, *4*, 4062–4071. [[CrossRef](#)]

52. Zhao, K.; Wang, X.; Chen, T.; Wu, H.; Li, J.; Yang, B.; Li, D.; Wei, J. Bisphenol A Adsorption Properties of Mesoporous $\text{CaSiO}_3@SiO_2$ Grafted Nonwoven Polypropylene Fiber. *Ind. Eng. Chem. Res.* **2017**, *56*, 2549–2556. [[CrossRef](#)]
53. Wang, Z.; Zhang, P.-B.; Hu, F.; Zhao, Y.; Zhu, L.-P. A crosslinked β -cyclodextrin polymer used for rapid removal of a broad-spectrum of organic micropollutants from water. *Carbohydr. Polym.* **2017**, *177*, 224–231. [[CrossRef](#)] [[PubMed](#)]

Publisher's Note: MDPI stays neutral with regard to jurisdictional claims in published maps and institutional affiliations.



© 2020 by the authors. Licensee MDPI, Basel, Switzerland. This article is an open access article distributed under the terms and conditions of the Creative Commons Attribution (CC BY) license (<http://creativecommons.org/licenses/by/4.0/>).